Figures and figure supplements

Arp2/3 complex activity enables nuclear YAP for naïve pluripotency of human embryonic stem cells

Nathaniel Paul Meyer *et al*.

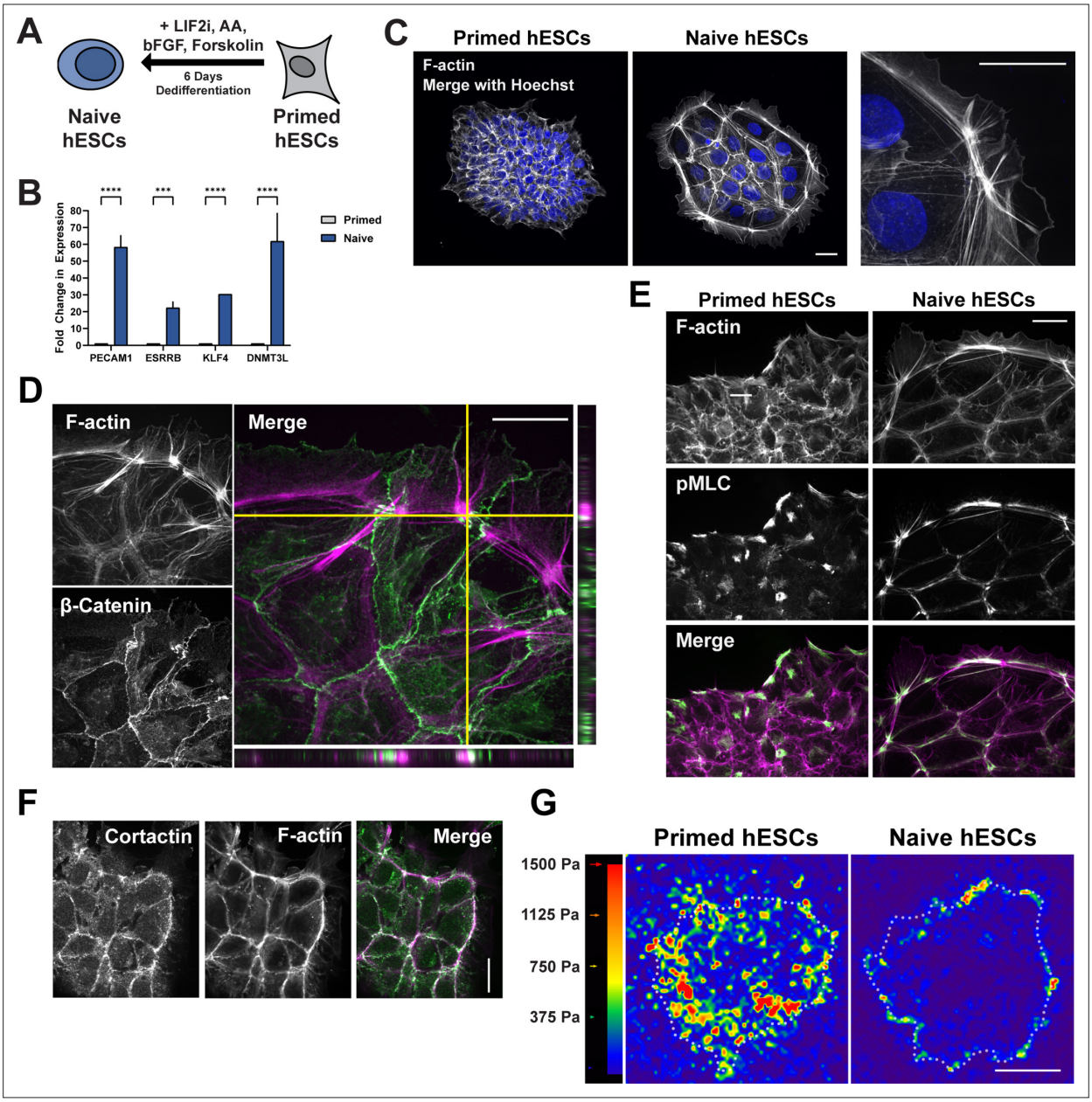

Figure 1. Dedifferentiation of primed human embryonic stem cells (hESCs) to naïve pluripotency includes F-actin filament remodeling and the formation of an actin ring. (**A**) Schematic of the dedifferentiation process from primed to naïve hESCs. (**B**) Confirmation of dedifferentiation indicated by increased expression of pluripotency genes associated with a naïve state as determined by quantitative PCR (qPCR). Data represent the means ± SD normalized to Oct4 (n=3 separate cell preparations). Two-way ANOVA with Tukey post hoc test was used to compare between groups. (**C–G**) Images of primed and naïve stem cells stained or immunolabeled for actin cytoskeleton components. (**C**) Confocal (left and middle) and super-resolution (right) images of hESCs stained for F-actin with phalloidin (white) and Hoechst (blue) show a bundled actin filament ring around colonies of naïve but not primed cells. (**D–F**) Confocal images of naïve hESCs immunolabeled for β-catenin (**D**), phosphorylated myosin light chain (pMLC) (**E**), and cortactin (**F**) and stained for F-actin with phalloidin (magenta) to characterize the actin filament ring. Scale bars, 25 μM. (**G**) Representative stress maps generated by traction force microscopy (TFM). Dotted outlines indicate colony boarders. Scale bar, 50 μM.

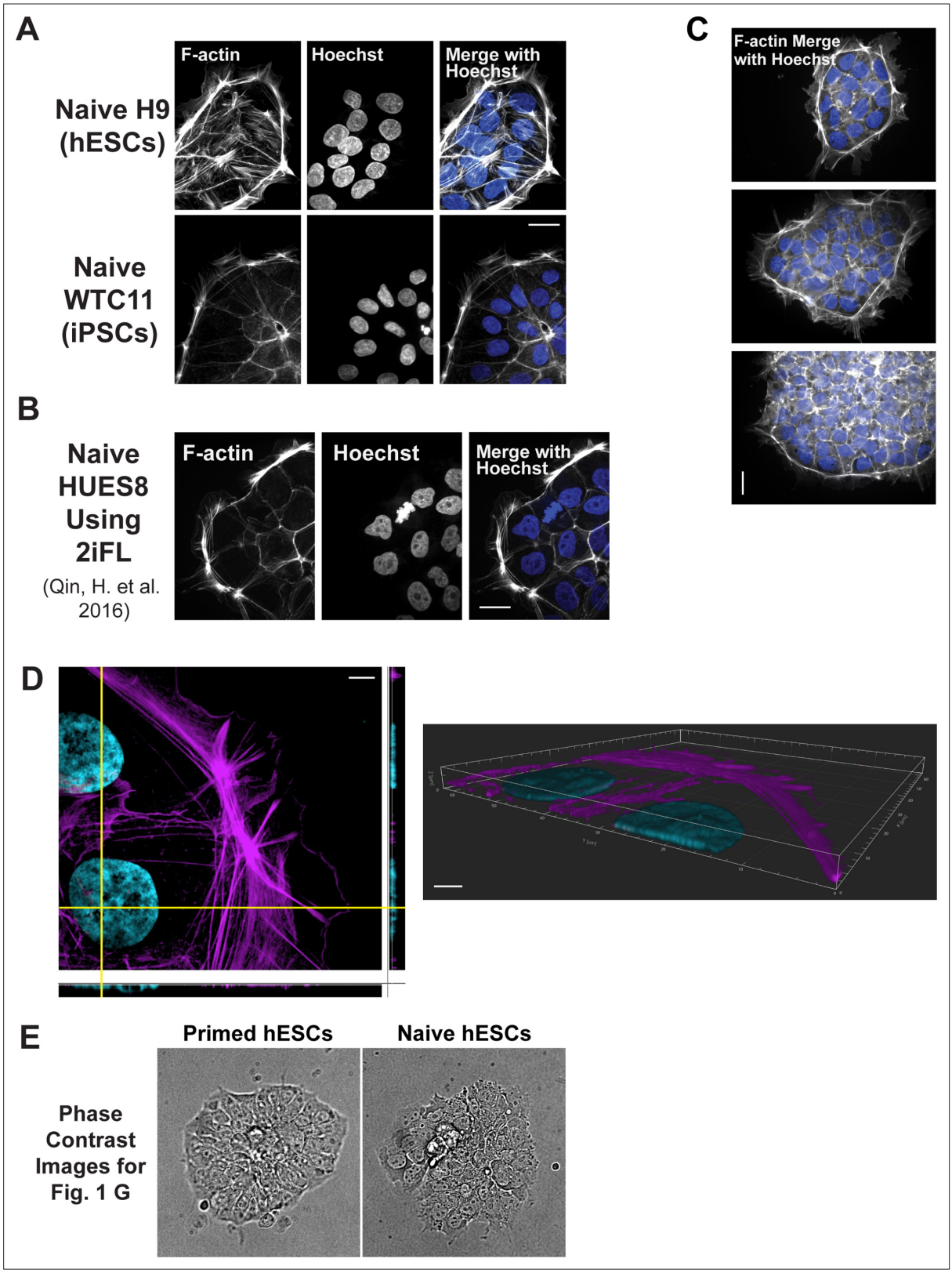

Figure 1—figure supplement 1. The actin ring architecture forms independent of cell line, dedifferentiation media, and colony size. (**A**) Confocal images of naïve H9 human embryonic stem cells (hESCs) and WTC11 induced pluripotent stem cells (iPSCs) stained for F-actin with phalloidin. (**B**) Confocal images of naïve hESCs using an alternative dedifferentiation medium (***Qin et al., 2016***). (**C**) Confocal images of naïve hESCs at different colony sizes. (**D**) Super-resolution images of hESCs stained for F-actin with phalloidin (magenta) and Hoechst (cyan). Orthogonal views (left panels)

Figure 1—figure supplement 1 continued on next page

Figure 1—figure supplement 1 continued

in conjunction with 3D reconstruction (right panel) demonstrate the 3D architecture of the actin ring in naïve colonies. (**E**) Phase contrast images of colonies used to show representative tractions for traction force microscopy in ***Figure 1G***. Images are representative from at least three separate determinations. Scale bars, 25 μM.

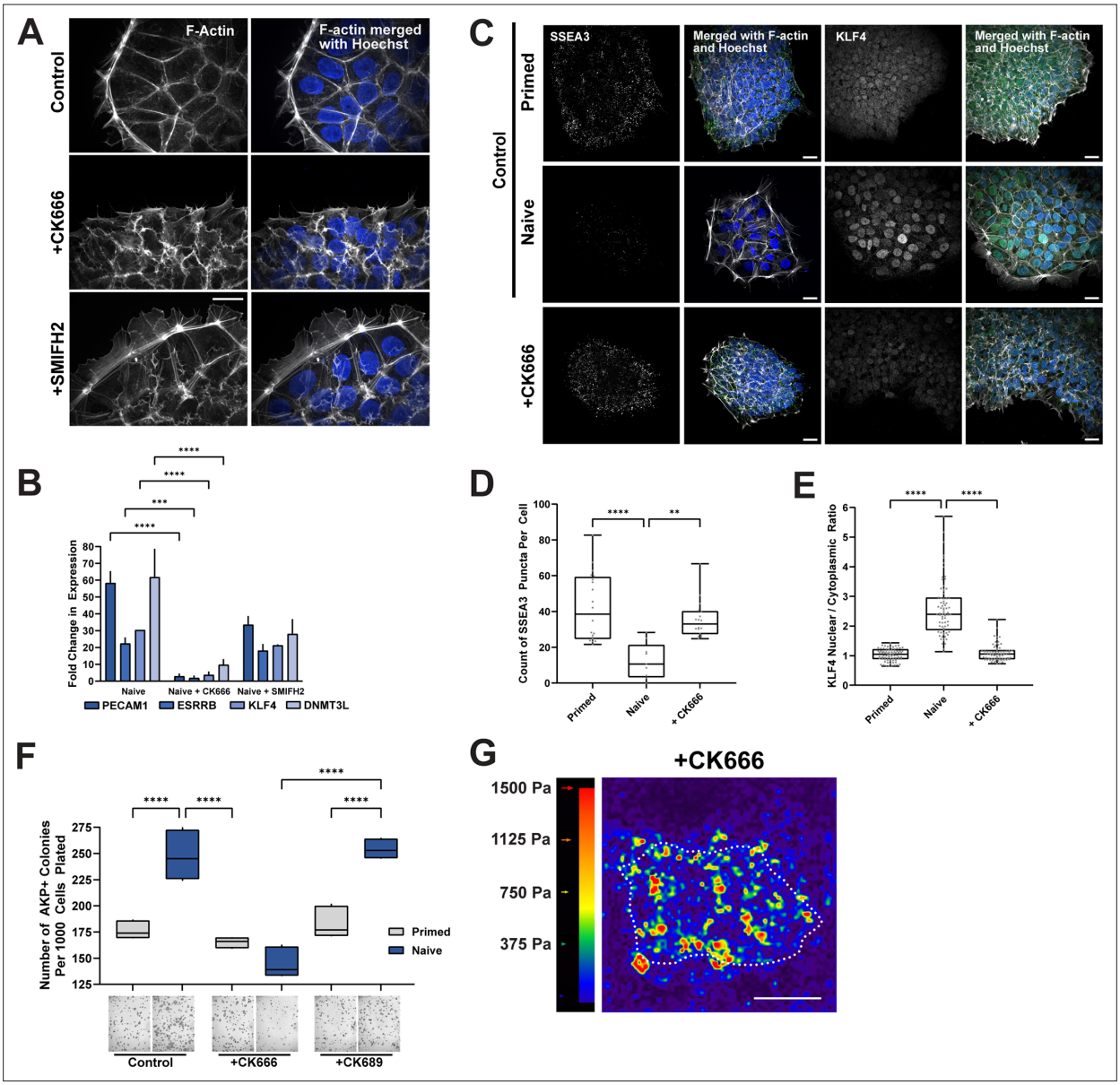

Figure 2. Inhibiting Arp2/3 complex but not formin activity blocks formation of an actin ring and dedifferentiation to naïve pluripotency. (**A**) Confocal images of D6 naïve human embryonic stem cells (hESCs) maintained in the absence (Control) or presence of 80 μM CK666 or 50 μM SMIFH2 and stained for F-actin with phalloidin and nuclei with Hoechst. (**B**) Expression of the indicated pluripotency transcripts determined by quantitative PCR (qPCR) at D6 of dedifferentiation in the absence (Control) or presence of CK666 or SMIFH2. The Arp2/3 complex activity inhibitor CK666 impairs upregulation of pluripotency genes used to identify naïve pluripotency. Data are the means ± SD of three determinations normalized to Oct4. Two-way ANOVA with Tukey post hoc test was used to compare between groups. (**C–E**) Confocal images of control primed and naïve hESCs and D6 cells dedifferentiated in the presence of CK666 immunolabeled for the primed marker SSEA3, quantified in (**D**) and the naïve marker KLF4, quantified in (**E**). Box plots in (**D**) and (**E**) show median, first and third quartile, with whiskers extending to observations within 1.5 times the interquartile range. (**F**) Clonogenicity, determined by alkaline phosphatase positive colonies (quantified in top panel and representative brightfield images in bottom panel) in control primed and naïve hESC as well as dedifferentiated in the presence of CK666 or 80 μM CK689, an inactive analog of CK666. Data are the means ± SD normalized to the number of cells plated in three separate determinations. Box plots are as described in (**D, E**) and one-way ANOVA with Tukey post hoc test was used to compare between groups. Scale bars, 25 μM. (**G**) Representative stress maps generated by traction force microscopy (TFM). Dotted outlines indicate colony boarders. Scale bar, 50 μM.

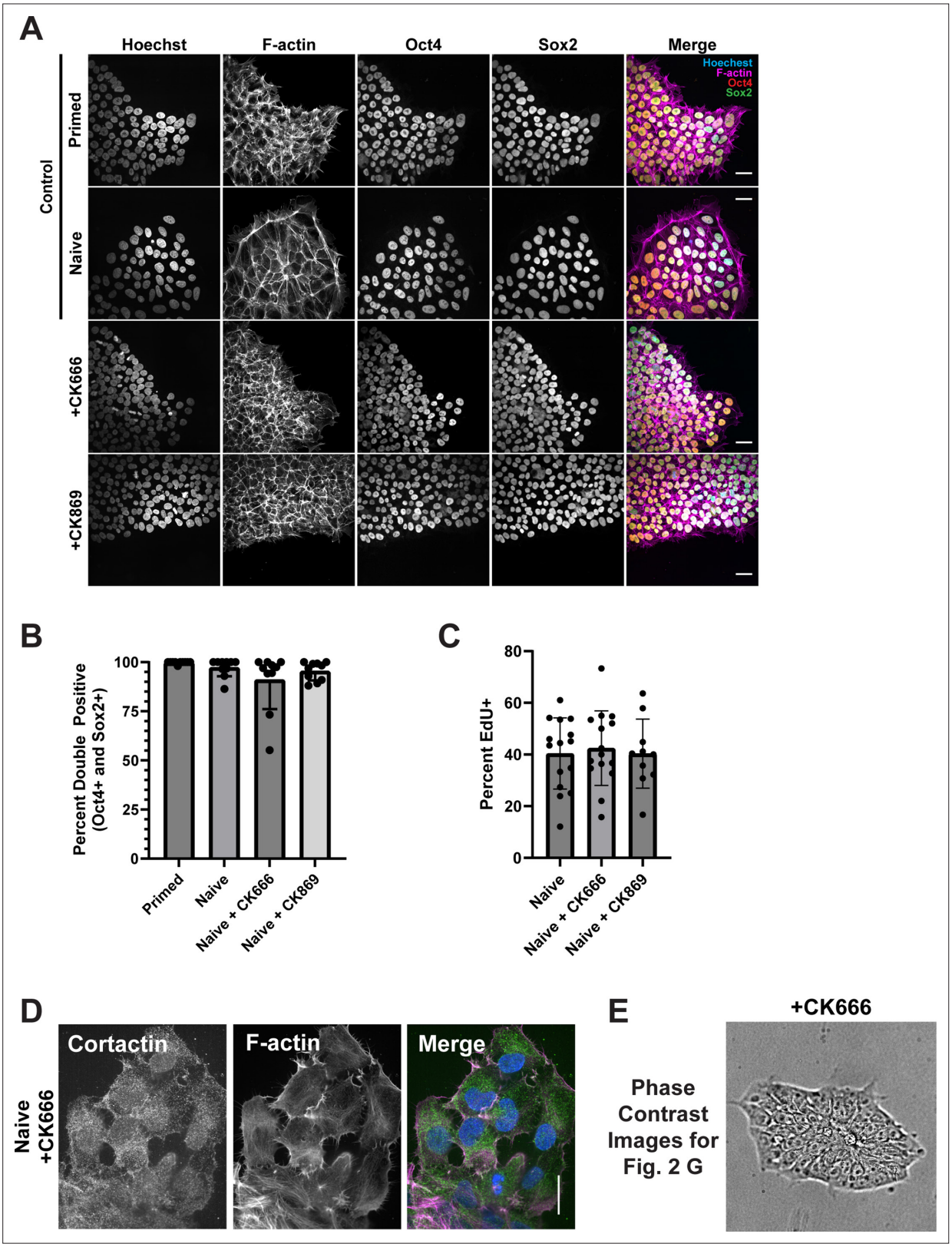

Figure 2—figure supplement 1. Inhibiting Arp2/3 complex activity in hESCs does not lead to an exit from pluripotency and does not alter rates of proliferation. (**A**) Confocal images of D6 naïve human embryonic stem cells (hESCs) treated with or without CK666 or CK869 stained for F-actin with phalloidin (magenta) and Hoechst (blue) and immunolabeled for pluripotency markers Oct4 (red) and Sox2 (green). (**B**) Quantification of cells double positive for Oct4 and Sox2. (**C**) Quantification of EdU+ cells after a 1 hr pulse of EdU. Data in (**A, B, C**) are the means ± SD normalized to the number of

Figure 2—figure supplement 1 continued on next page

Figure 2—figure supplement 1 continued

cells plated from three separate determinations. One-way ANOVA with Tukey post hoc test was used to compare between groups for data in (**B, C**); no significant differences were found. (**D**) Confocal images of naïve hESCs treated with CK666 and stained for cortactin (green) and F-actin (magenta). (**E**) Phase contrast images of colonies used to show representative tractions for traction force microscopy in ***Figure 2G***. Images are representative from at least three separate determinations. Scale bars, 25 μM.

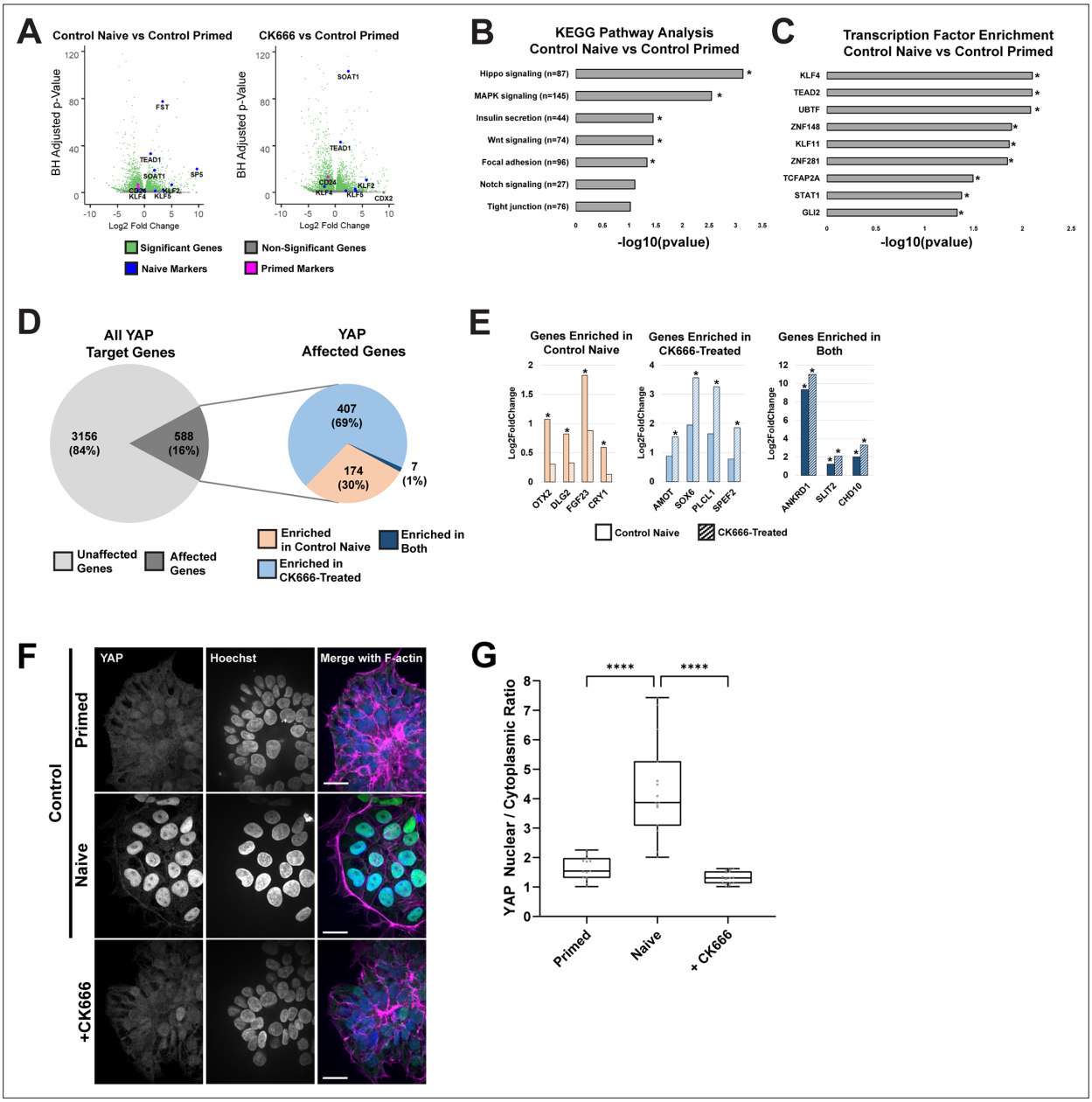

Figure 3. Inhibiting Arp2/3 complex activity disrupts Hippo signaling in naïve human embryonic stem cells (hESCs). (**A**) Volcano plots showing transcriptome fold-changes (padj) of dedifferentiations in the absence (Control Naïve) or presence of CK666-treated dedifferentiations compared with primed hESCs. Each dot represents a single gene, with significant genes (padj<0.05; false discovery rate [FDR]-corrected by Benjamini-Hochberg procedure) in green. Notable primed and naïve markers are depicted in magenta and blue, respectively. (**B, C**) KEGG pathway analysis (**B**) and transcription factor enrichment analysis (**C**) of control primed and naïve hESCs. The number of differentially expressed genes (DEGs) indicated in each pathway is displayed and asterisks indicate significantly enriched pathways (p<0.05). (**D**) Unbiased screening of all known YAP target genes in dedifferentiated cells in the absence (Control Naive) and presence of CK666. Affected genes were further analyzed to indicate whether they are enriched in control, CK666-treated, or both conditions when compared with primed controls. (**E**) Expression of selected YAP target genes from bulk RNA-sequencing (RNAseq), with asterisks indicating significant difference (padj<0.05). (**F**) Representative confocal images of control primed and naïve hESCs and naïve hESCs generated in the presence of 80 μM CK666 immunolabeled for YAP and stained for nuclei with Hoechst and F-actin with phalloidin. (**G**) Quantification of nuclear to cytoplasmic ratio of YAP from images as shown in (**F**). Box plots show median, first and third quartile, with whiskers extending to observations within 1.5 times the interquartile range. Data are from five separate cell preparations and one-way ANOVA with Tukey post hoc test was used to compare between groups. Scale bars, 25 μM.

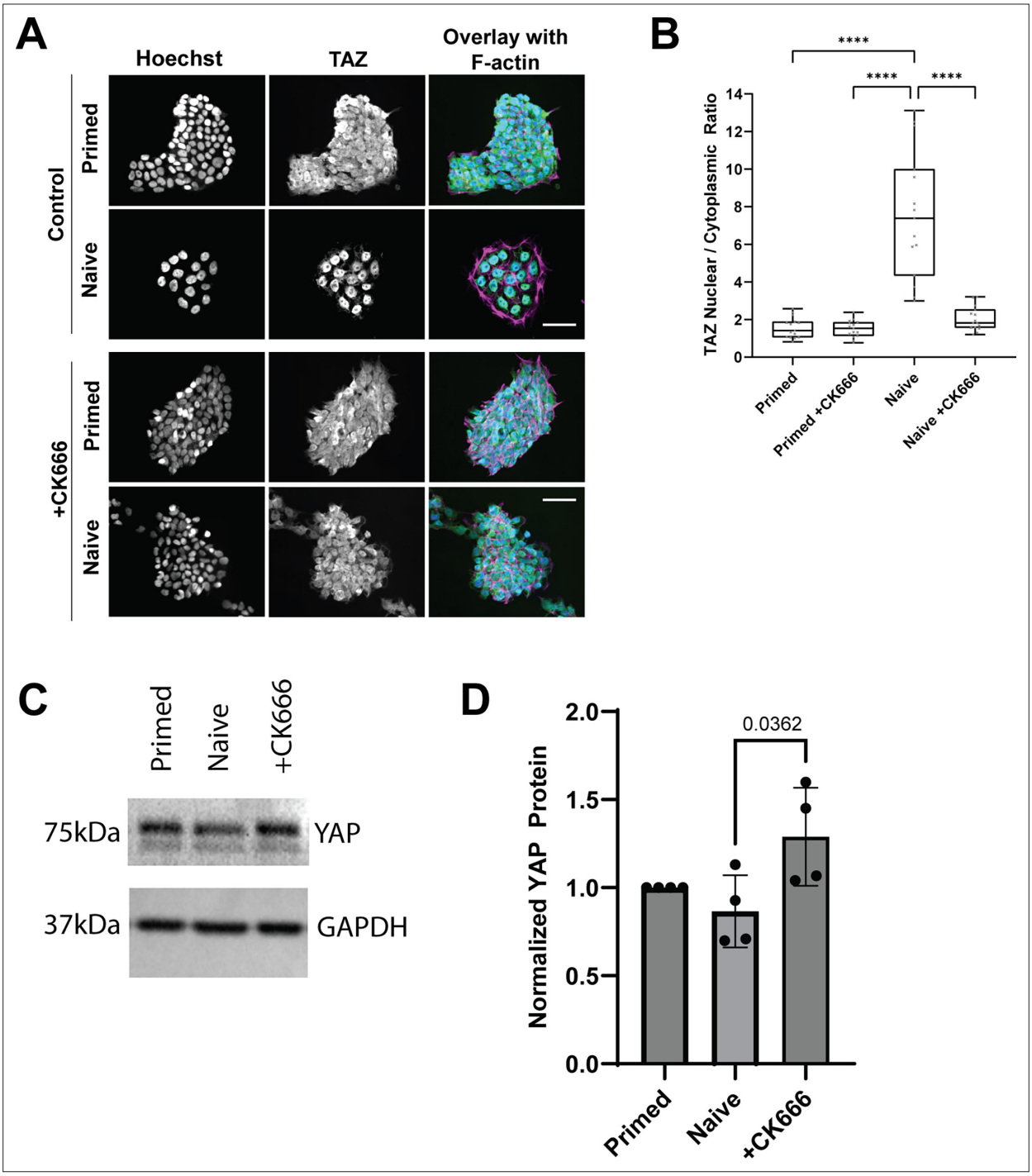

Figure 3—figure supplement 1. Inhibiting Arp2/3 complex activity disrupts TAZ localization in naïve hESCs. (**A**) Confocal images of D6 primed and naïve human embryonic stem cells (hESCs) in the absence (Control) or presence of 80 μM CK666 immunolabled for TAZ (green) and stained for F-actin with phalloidin (magenta) and Hoechst (blue). (**B**) Quantification of nuclear to cytoplasmic ratio of TAZ from images shown in (**A**). Box plots show median, first and third quartile, with whiskers extending to observations within 1.5 times the interquartile range. Data are from five separate cell preparations and one-way ANOVA with Tukey post hoc test was used to compare between groups. Images are representative from at least three separate determinations. Scale bars, 25 μM. (**C, D**) Representative immunoblot of total YAP in cell lysates (**C**) and quantification (**D**) of total YAP in immunoblots from three separate cell preparations. Data are from three separate cell preparations and one-way ANOVA with Tukey post hoc test was used to compare between groups.

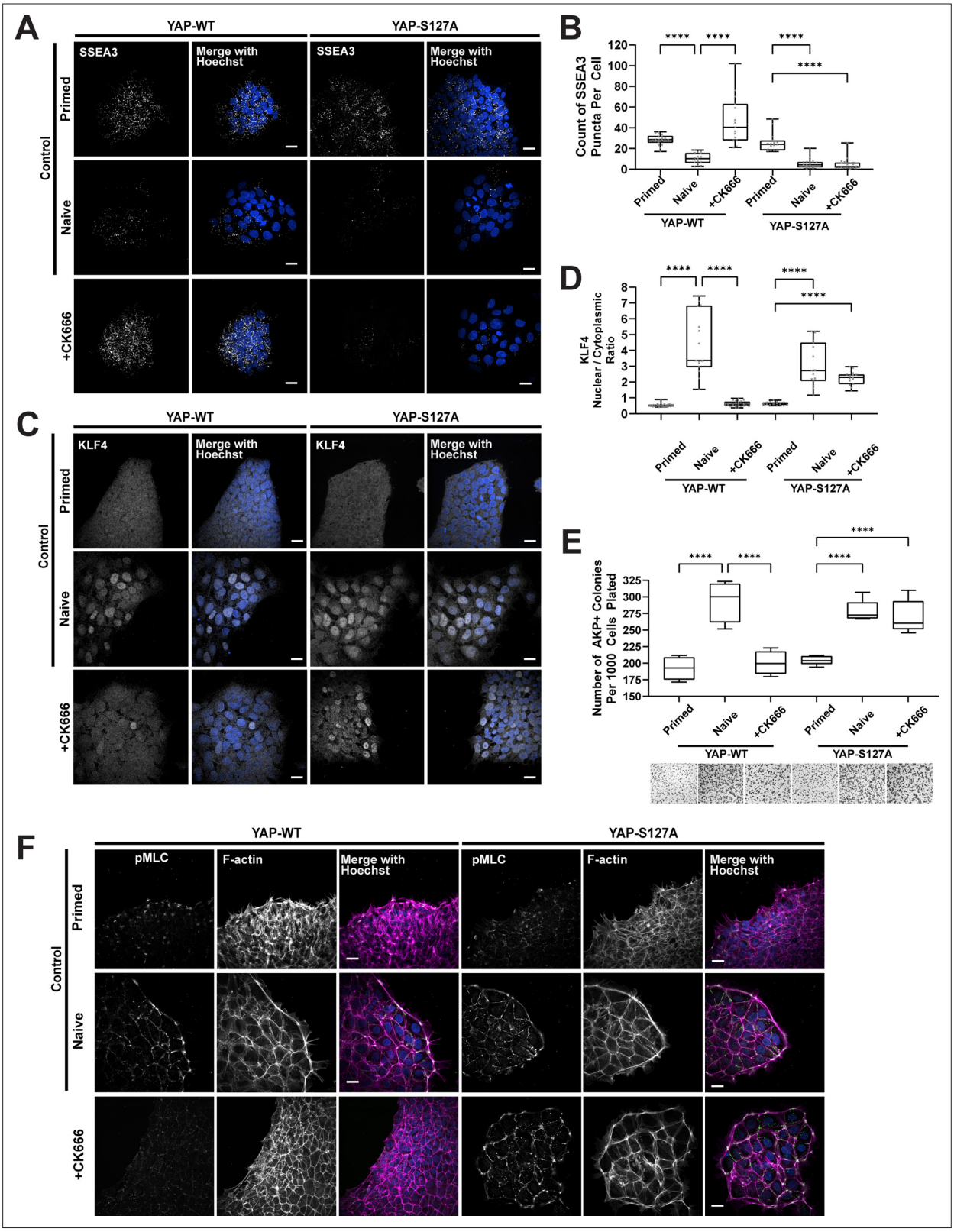

Figure 4. Overexpression of YAP-S127A rescues naïve pluripotency blocked with inhibiting Arp2/3 complex activity. (**A, C**) Representative confocal images of control primed, control naïve cells, and cells dedifferentiated in the presence of CK666 with or without stably overexpressing YAP-WT or YAP-S127A immunolabeled for the primed marker SSEA3 (**A**) or the naïve marker KLF4 (**C**) and stained for nuclei with Hoechst and F-actin with phalloidin. (**B, D**) Images as in (**A**) and (**C**) were used to quantify, respectively, the number of SSEA3 puncta (**B**) and the nuclear to cytoplasmic ratio of KLF4 (**D**). Box

Figure 4 continued on next page

Figure 4 continued

are plots as described for ***Figure 2***. (**E**) Clonogenicity, determined by alkaline phosphatase positive colonies (quantified in top panel and representative brightfield images in bottom panel) in control primed and naïve human embryonic stem cell (hESC), and dedifferentiated in the presence of CK666 with stably expressed YAP WT or YAP-S127A. Data are the means ± SD normalized to the number of cells plated from five separate determinations, with box plots as described for ***Figure 2d and e*** and one-way ANOVA with Tukey post hoc test was used to compare between groups. Representative confocal images of control primed, control naïve cells, and cells dedifferentiated in the presence of CK666 with or without stably expressing YAP-WT or YAP-S127A immunolabeled for phosphorylated myosin light chain (pMLC) and stained for nuclei with Hoechst and F-actin with phalloidin. Scale bars, 25 μM.